https://doi.org/10.1038/s41586-018-0848-x

Large influence of soil moisture on long-term terrestrial carbon uptake

Julia K. Green[1]*, Sonia I. Seneviratne[2], Alexis M. Berg[3], Kirsten L. Findell[4], Stefan Hagemann[5], David M. Lawrence[6] & Pierre Gentine[1,7]

Although the terrestrial biosphere absorbs about 25 per cent of anthropogenic carbon dioxide (CO_2) emissions, the rate of land carbon uptake remains highly uncertain, leading to uncertainties in climate projections[1,2]. Understanding the factors that limit or drive land carbon storage is therefore important for improving climate predictions. One potential limiting factor for land carbon uptake is soil moisture, which can reduce gross primary production through ecosystem water stress[3,4], cause vegetation mortality[5] and further exacerbate climate extremes due to land–atmosphere feedbacks[6]. Previous work has explored the impact of soil-moisture availability on past carbon-flux variability[3,7,8]. However, the influence of soil-moisture variability and trends on the long-term carbon sink and the mechanisms responsible for associated carbon losses remain uncertain. Here we use the data output from four Earth system models[9] from a series of experiments to analyse the responses of terrestrial net biome productivity to soil-moisture changes, and find that soil-moisture variability and trends induce large CO_2 fluxes (about two to three gigatons of carbon per year; comparable with the land carbon sink itself[1]) throughout the twenty-first century. Subseasonal and interannual soil-moisture variability generate CO_2 as a result of the nonlinear response of photosynthesis and net ecosystem exchange to soil-water availability and of the increased temperature and vapour pressure deficit caused by land–atmosphere interactions. Soil-moisture variability reduces the present land carbon sink, and its increase and drying trends in several regions are expected to reduce it further. Our results emphasize that the capacity of continents to act as a future carbon sink critically depends on the nonlinear response of carbon fluxes to soil moisture and on land–atmosphere interactions. This suggests that the increasing trend in carbon uptake rate may not be sustained past the middle of the century and could result in accelerated atmospheric CO_2 growth.

The vast divergence in terrestrial carbon-flux projections from Earth system models (ESMs) reflects both the difficulty of observing and modelling biogeochemical cycles, as well as the uncertainty in the response of ecosystems to rising atmospheric CO_2[1,2]. Rising atmospheric CO_2 can generate a fertilization effect that initially increases the rates of photosynthesis and terrestrial CO_2 uptake[10]. However, this fertilization effect may saturate in the future if the maximum ecosystem photosynthesis rate is achieved or because of other limiting factors, such as nutrient limitation[11].

Here we demonstrate that the net biome productivity (NBP) response to soil-moisture variability is not a zero-sum game. Reductions in NBP driven by strong dry soil-moisture anomalies (through increased water stress, fire frequency and intensity, and heat stress) are not compensated by increased NBP under anomalously wet conditions. Additionally, drying soil-moisture trends can transition an ecosystem of high biomass (for example, a forest) to an ecosystem of lower biomass (for example, a grassland), thus accounting for further reductions in NBP[12].

Using the data of four models from the Global Land–Atmosphere Coupling Experiment Coupled Model Intercomparison Project phase 5

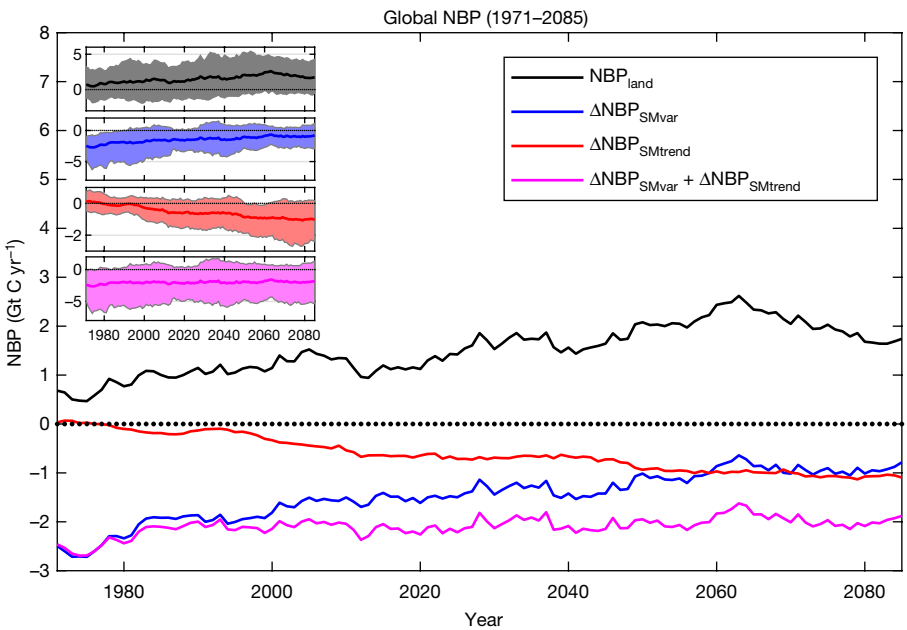

Fig. 1 | Global NBP during the twenty-first century. The evolution of total global NBP (NBP_{land}), along with changes in NBP that can be attributed to soil-moisture variability (NBP_{SMvar}) and trend ($NBP_{SMtrend}$) through the twenty-first century. The shaded areas in the insets show the spread of the results of the four models for each of the NBP components.

[1]Department of Earth and Environmental Engineering, Columbia University, New York, NY, USA. [2]Department of Environmental Systems Science, ETH Zurich, Zurich, Switzerland. [3]Department of Civil and Environmental Engineering, Princeton University, Princeton, NJ, USA. [4]Geophysical Fluid Dynamics Laboratory, Princeton, NJ, USA. [5]Institute of Coastal Research, Helmholtz-Zentrum Geesthacht, Geesthacht, Germany. [6]Climate and Global Dynamics Laboratory, Terrestrial Sciences, National Center for Atmospheric Research, Boulder, CO, USA. [7]The Earth Institute, Columbia University, New York, NY, USA. *e-mail: jg3405@columbia.edu

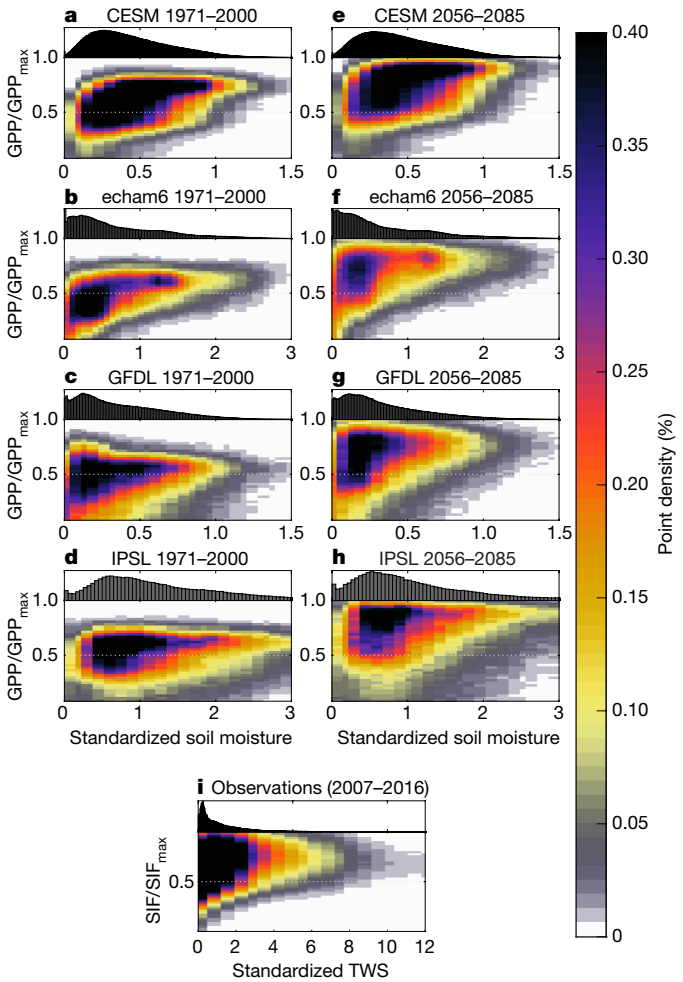

Fig. 2 | Biosphere photosynthetic activity response curves. **a**–**h**, Normalized growing-season GPP versus standardized soil moisture for the baseline (1971–2000; **a**–**d**) and a future period (2056–2085; **e**–**h**) in the GLACE-CMIP5 reference scenario. **i**, Normalized and detrended observational solar-induced fluorescence (SIF; a proxy for photosynthesis) versus standardized total water storage (TWS; the sum of soil moisture and groundwater, surface water, snow and ice) from the Gravity Recovery and Climate Experiment (GRACE; 2007–2016). The probability density functions of the soil-moisture and TWS data are plotted at the top. Details of the observational data and the normalization and standardizations of all datasets can be found in Methods.

(GLACE-CMIP5)[9] (Extended Data Table 1), we isolate the changes in global terrestrial NBP (NBP_{land}) due to soil-moisture variations from the climatological annual cycle (NBP_{SMvar}) and to longer-term soil-moisture trends ($NBP_{SMtrend}$); see Methods. These experiments allow the systematic quantification of the effect of moisture across models. For each model, the same sea surface temperatures and radiative forcing agents (which are based on historical and Representative Concentration Pathway 8.5 (RCP8.5) coupled simulations) are prescribed in all runs. These experiments uniquely allow us to isolate the role of soil-moisture dynamics in the climate system. Previous studies have used these experiments to evaluate various aspects of land–atmosphere interactions, including enhanced extremes and aridity[9,13,14].

Although the models give quantitatively different simulated soil-moisture results, they show robust qualitative agreement on the strong effect of soil moisture on NBP (Fig. 1). Across models, soil-moisture variability and trends in the mean moisture state strongly reduce the land carbon sink, with their combined effect ($NBP_{SMvar} + NBP_{SMtrend}$) being of the same order of magnitude as the land sink (NBP_{land}, estimated from the reference (CTL) runs; Fig. 1). It should be noted that in contrast to the global carbon budget[1], the land sink term defined by NBP includes emissions from land use and land cover change.

Soil-moisture variability alone reduces the global terrestrial sink by over twice its absolute magnitude (about 2.5 Gt C yr^{-1}) at the start of the study period, and by more than half its absolute magnitude (about 0.8 Gt C yr^{-1}) at the end of the twenty-first century (NBP_{SMvar}) (Fig. 1). Previous studies have shown that soil-moisture variability induced by extreme events (such as droughts and heatwaves) can explain a large fraction of the interannual variability in carbon fluxes[7,15,16]. Here we show that beyond impacts on interannual anomalies, soil-moisture variability substantially reduces the mean long-term (multi-year) land CO_2 uptake.

These reductions are due to the nonlinear response of vegetation carbon uptake to water stress: photosynthesis sharply drops off once an ecosystem becomes water-limited in models, which is supported by observational data (Fig. 2, Extended Data Fig. 1). These carbon losses are not recovered during periods with a (similar-amplitude) positive moisture anomaly. Indeed, dryness reduces evaporation and therefore surface cooling[17], which results in increases in temperature and vapour pressure deficit (VPD) (Extended Data Figs. 2, 3) due to soil moisture–atmosphere feedbacks[13,18]. These feedbacks further reduce photosynthesis through their effect on vegetation stomatal closure. Although respiration also decreases with soil moisture (Extended Data Figs. 4 and 5), the land–atmosphere increase in temperature increases the ratio of respiration to gross primary production (GPP; Fig. 3), leading to an overall strong NBP reduction with soil moisture (Fig. 1). In addition, NBP is further reduced by fires during hot and dry spells from the increased prevalence of dead litter from tree mortality and foliage loss as fire fuel[12,19].

During the baseline period (1971–2000), the reduction in the mean terrestrial carbon sink caused by soil-moisture variability is globally widespread (Fig. 4, Extended Data Fig. 1). There are large NBP reductions in seasonally dry climates (western United States and Central Europe), tropical savannahs (Brazil, India and northern Australia), and semi-arid/monsoonal regions (the Sahel, South Africa and eastern Australia) that are known to be water-limited ecosystems and have been shown to be the main drivers of interannual terrestrial CO_2 flux variability[7,8]. In the future (2056–2085), negative impacts on mean NBP will remain strong in semi-arid (for example, the Sahel), humid (such as the south-eastern United States and Colombia) and monsoonal (for example, India and northern Australia) climates.

Long-term soil-moisture trends, which display a gradual drying in most areas (except in some areas of the tropics[9,13]; Extended Data Fig. 6), will reduce the global terrestrial sink by over two thirds of its absolute magnitude (about 1.1 Gt C yr^{-1}) at the end of the twenty-first century ($NBP_{SMtrend}$; Fig. 1). Regions showing the strongest negative impacts are semi-arid regions bordering deserts (eastern Australia, northern Sahel and northern Mexico), humid subtropical climates (eastern China and southern Brazil) and Mediterranean Europe (Fig. 4). Under enhanced greenhouse-gas forcing within the twenty-first century, it is expected that these regions will become more strongly water-limited[6,20], which will result in the simulated drop in GPP shown in Extended Data Fig. 1.

The evolution of NBP_{SMvar} and $NBP_{SMtrend}$ through the twenty-first century can be explained by several concurring mechanisms. First, increased vegetation water-use efficiency due to carbon fertilization effects[21] (Extended Data Fig. 7) makes ecosystems more resistant to a negative soil-moisture anomaly. Second, an ecosystem can have decreased NBP response owing to the vegetation already being in a severely water-stressed environment—in other words, the overall global drying trend in soil moisture shifts several ecosystems into arid conditions, which reduces the influence of the temporal variability of soil moisture on NBP. Third, insufficient drought recovery time for an ecosystem can shift a forest ecosystem to a grassland (storing less carbon[5]; Extended Data Fig. 8), and thus an NBP loss from a dry year is not necessarily compensated by a wet year (Fig. 2).

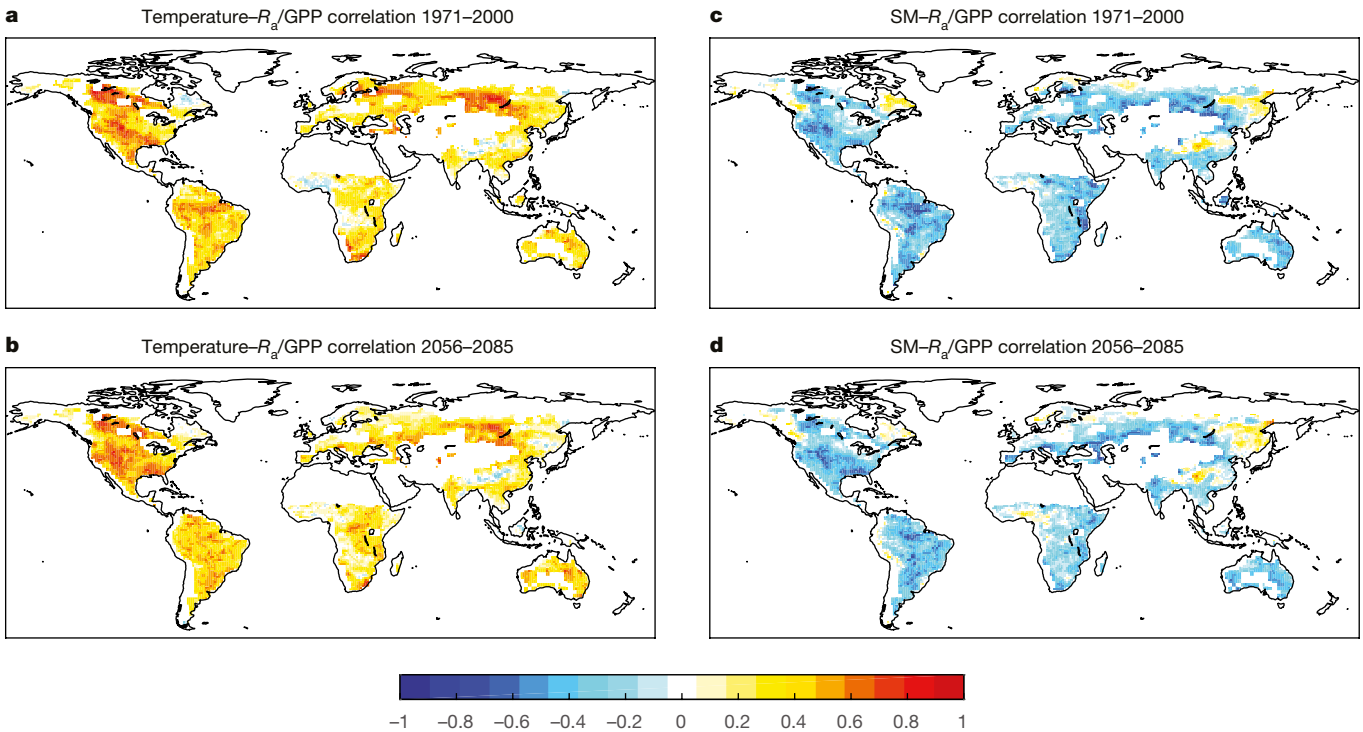

Fig. 3 | Correlations of the ratio of autotrophic respiration (R_a) to GPP. **a**, **b**, Correlations of R_a/GPP with temperature during the baseline (1971–2000; **a**) and a future modelled period (2056–2085; **b**). **c**, **d**, Correlations of R_a/GPP with soil moisture (SM) during the baseline (1971–2000; **c**) and a future period (2056–2085; **d**). All data are from the GLACE-CMIP5 CTL run.

Despite the cumulative negative impact of these soil-moisture effects on global NBP ($NBP_{SMvar} + NBP_{SMtrend}$), NBP_{land} (the mean of the four GLACE-CMIP5 models) remains a sink throughout the study period, mainly owing to the effects of carbon fertilization[10]. This is due to the strong simulated response of the tropics to increases in CO_2 (Extended Data Fig. 9), the lengthening of the growing seasons in mid- and northern latitudes due to increasing temperatures (Extended Data Fig. 2), as well as to reduced cloud coverage and associated increases in photosynthesis in energy-limited regions[22,23]. However, despite the continual increase in atmospheric CO_2 concentrations in the business-as-usual emission scenario, the modelled global carbon sink reaches a peak shortly after 2060, when the terrestrial biosphere will have

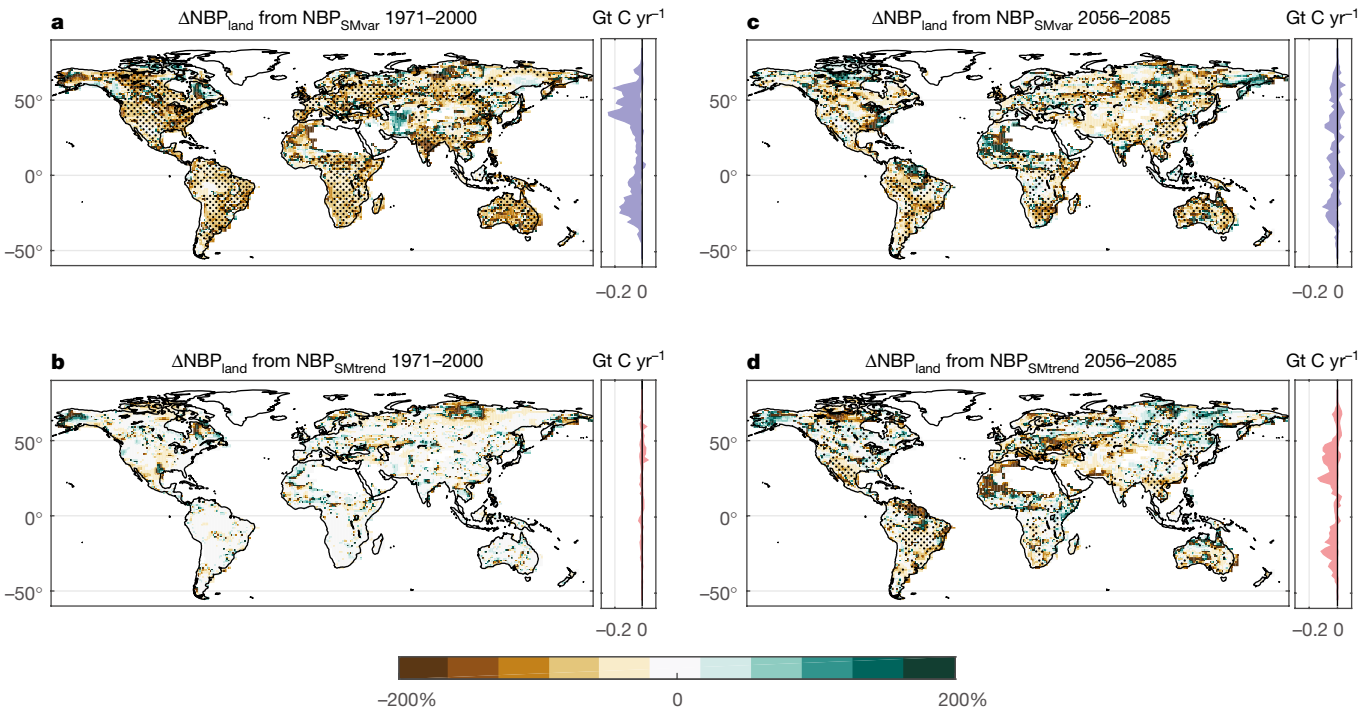

Fig. 4 | Regional NBP changes. a–d, Per cent changes in NBP (NBP_{land}) due to soil-moisture variability (NBP_{SMvar}) and trend ($NBP_{SMtrend}$) during the baseline (1971–2000; **a**, **b**) and a future period (2056–2085; **c**, **d**). Stippling highlights regions where the three models agree on the sign of the change. The latitudinal NBP subplots on the right show how these NBP changes translate to an overall NBP magnitude across latitudes. The thick line in each subplot represents the model mean and the shaded areas show the model spread.

apparently reached its maximum carbon absorption rate, in agreement with a wider range of ESM predictions[24].

Whether the effect of carbon fertilization on the global carbon sink is overpredicted by models is unclear, owing to the lack of long-term experiments; there has been, however, evidence that the initial increase in photosynthesis rates observed in C3 plants (about 97% of plant species) may actually reverse after 15–20 years[25]. Additionally, many of the factors limiting carbon fertilization have large uncertainties or are not well represented in models; thus the magnitude of the land carbon sink presented here is probably too high. For example, many studies of free-air CO_2 enrichment have shown limited or no response to increased CO_2 concentration levels because of nutrient limitations[26]. Only one of the four GLACE-CMIP5 models (CESM; Community Earth System Model) includes the interaction of the nitrogen and carbon cycles and has CO_2 fertilization rates much lower than the other models (Extended Data Fig. 10). A reduced CO_2 fertilization effect would mean that our finding regarding the negative effects of soil-moisture variability on NBP would be proportionally larger and have a greater potential of turning the land to a carbon source during the twenty-first century.

On the basis of our findings it appears critical to correctly assess and simulate the (nonlinear) dependence of GPP and NBP on soil-moisture variability in ESMs, as well as the associated land–atmosphere feedbacks. However, most current models only include stomatal limitations on photosynthesis[27] and implement empirical formulations of water-stress functions related to soil water content and VPD[28]. They have high degrees of uncertainty associated with their representation of canopy conductance, especially in dry environments[29], and do not include several important plant water-stress processes related to plant hydraulics, such as xylem embolism[30]. It has been shown that the vegetation sensitivity to water availability, even within a single plant functional type, can vary between a factor of 3 and 5 during drought, resulting in large variations of plant response and/or mortality to droughts[30]. Additionally, drought legacy effects, which can last for several years, and drought-related plant mortality are not included in ESMs[31]. Finally, the strength of land–atmosphere interactions is underestimated in models[32], with potential important implications for VPD and temperature. By quantifying the critical importance of soil-water variability for the terrestrial carbon cycle, our results highlight the necessity of implementing improved, mechanistic representations of vegetation response to water stress and land–atmosphere coupling in ESMs to constrain the future terrestrial carbon flux and to better predict future climate.

Online content

Any methods, additional references, Nature Research reporting summaries, source data, statements of data availability and associated accession codes are available at https://doi.org/10.1038/s41586-018-0848-x.

Received: 5 March 2018; Accepted: 21 November 2018;
Published online 23 January 2019.

1. Le Quéré, C. et al. Global carbon budget 2017. *Earth Syst. Sci. Data* **10**, 405–448 (2018).
2. Ballantyne, A. P. et al. Audit of the global carbon budget: estimate errors and their impact on uptake uncertainty. *Biogeosciences* **12**, 2565–2584 (2015).
3. Zhao, M. & Running, S. W. Drought-induced reduction in global terrestrial net primary production from 2000 through 2009. *Science* **329**, 940–943 (2010).
4. Humphrey, V. et al. Sensitivity of atmospheric CO_2 growth rate to observed changes in terrestrial water storage. *Nature* **560**, 628–631 (2018).
5. Schwalm, C. R. et al. Global patterns of drought recovery. *Nature* **548**, 202–205 (2017).
6. Seneviratne, S. I. et al. Investigating soil moisture-climate interactions in a changing climate: a review. *Earth Sci. Rev.* **99**, 125–161 (2010).
7. Poulter, B. et al. Contribution of semi-arid ecosystems to interannual variability of the global carbon cycle. *Nature* **509**, 600–603 (2014).
8. Ahlström, A. et al. The dominant role of semi-arid ecosystems in the trend and variability of the land CO_2 sink. *Science* **348**, 895–899 (2015).
9. Seneviratne, S. I. et al. Impact of soil moisture–climate feedbacks on CMIP5 projections: first results from the GLACE-CMIP5 experiment. *Geophys. Res. Lett.* **40**, 5212–5217 (2013).
10. Schimel, D., Stephens, B. B. & Fisher, J. B. Effect of increasing CO_2 on the terrestrial carbon cycle. *Proc. Natl Acad. Sci. USA* **112**, 436–441 (2015).
11. Wieder, W. R., Cleveland, C. C., Smith, W. K. & Todd-Brown, K. Future productivity and carbon storage limited by terrestrial nutrient availability. *Nat. Geosci.* **8**, 441–444 (2015).
12. McDowell, N. G. & Allen, C. D. Darcy's law predicts widespread forest mortality under climate warming. *Nat. Clim. Change* **5**, 669–672 (2015).
13. Berg, A. et al. Land–atmosphere feedbacks amplify aridity increase over land under global warming. *Nat. Clim. Change* **6**, 869–874 (2016).
14. Lorenz, R. et al. Influence of land-atmosphere feedbacks on temperature and precipitation extremes in the GLACE-CMIP5 ensemble. *J. Geophys. Res. Atmos.* **121**, 607–623 (2016).
15. Schwalm, C. R. et al. Reduction in carbon uptake during turn of the century drought in western North America. *Nat. Geosci.* **5**, 551–556 (2012).
16. Reichstein, M. et al. Climate extremes and the carbon cycle. *Nature* **500**, 287–295 (2013).
17. Bateni, S. M. & Entekhabi, D. Relative efficiency of land surface energy balance components. *Wat. Resour. Res.* **48**, 1–8 (2012).
18. Seneviratne, S. I., Lüthi, D., Litschi, M. & Schär, C. Land-atmosphere coupling and climate change in Europe. *Nature* **443**, 205–209 (2006).
19. Brando, P. M. et al. Abrupt increases in Amazonian tree mortality due to drought-fire interactions. *Proc. Natl Acad. Sci. USA* **111**, 6347–6352 (2014).
20. Orlowsky, B. & Seneviratne, S. I. Elusive drought: uncertainty in observed trends and short-and long-term CMIP5 projections. *Hydrol. Earth Syst. Sci.* **17**, 1765–1781 (2013).
21. Greve, P., Roderick, M. L. & Seneviratne, S. I. Simulated changes in aridity from the last glacial maximum to $4\times CO_2$. *Environ. Res. Lett.* **12**, 114021 (2017).
22. Peñuelas, J. & Filella, I. Responses to a warming world. *Science* **294**, 793–795 (2001).
23. Nemani, R. R. et al. Climate-driven increases in global terrestrial net primary production from 1982 to 1999. *Science* **300**, 1560–1563 (2003).
24. Friedlingstein, P. et al. Uncertainties in CMIP5 climate projections due to carbon cycle feedbacks. *J. Clim.* **27**, 511–526 (2014).
25. Hovenden, M. & Newton, P. Plant responses to CO_2 are a question of time. *Science* **360**, 263–264 (2018).
26. Reich, P. B., Hobbie, S. E. & Lee, T. D. Plant growth enhancement by elevated CO_2 eliminated by joint water and nitrogen limitation. *Nat. Geosci.* **7**, 920–924 (2014).
27. Egea, G., Verhoef, A. & Vidale, P. L. Towards an improved and more flexible representation of water stress in coupled photosynthesis-stomatal conductance models. *Agric. For. Meteorol.* **151**, 1370–1384 (2011).
28. Verhoef, A. & Egea, G. Modeling plant transpiration under limited soil water: comparison of different plant and soil hydraulic parameterizations and preliminary implications for their use in land surface models. *Agric. For. Meteorol.* **191**, 22–32 (2014).
29. Franks, P. J., Berry, J. A., Lombardozzi, D. L. & Bonan, G. B. Stomatal function across temporal and spatial scales: deep-time trends, land-atmosphere coupling and global models. *Plant Physiol.* **174**, 583–602 (2017).
30. Konings, A. G., Williams, A. P. & Gentine, P. Sensitivity of grassland productivity to aridity controlled by stomatal and xylem regulation. *Nat. Geosci.* **10**, 284–288 (2017).
31. Anderegg, W. R. L. et al. Pervasive drought legacies in forest ecosystems and their implications for carbon cycle models. *Science* **349**, 528–532 (2015).
32. Green, J. K. et al. Regionally strong feedbacks between the atmosphere and terrestrial biosphere. *Nat. Geosci.* **10**, 410–414 (2017).

Acknowledgements This research was supported by a NASA Earth and Space Science Fellowship. We acknowledge the World Climate Research Programme (WCRP) Working Group on Coupled Modelling, which is responsible for CMIP, and we thank the climate modelling groups (listed in Extended Data Table 1 and Extended Data Figs. 9, 10) for producing and making available their model output. For CMIP the US Department of Energy's Program for Climate Model Diagnosis and Intercomparison provided coordinating support and led the development of software infrastructure, in partnership with the Global Organization for Earth System Science Portals. The GLACE-CMIP5 project was co-sponsored by WCRP's Global Energy and Water Exchanges Project (GEWEX) Land–Atmosphere System Study (GLASS) and the International Geosphere–Biosphere Programme (IGBP) Integrated Land–Ecosystem–Atmosphere Processes Study (ILEAPS). S.I.S. acknowledges the European Research Council (ERC) DROUGHT-HEAT project, funded by the European Commission's Seventh Framework Programme (grant agreement FP7-IDEAS-ERC-617518).

Reviewer information *Nature* thanks C. Schwalm, A. Verhoef and the other anonymous reviewer(s) for their contribution to the peer review of this work.

Author contributions J.K.G. wrote the main manuscript in collaboration with P.G. J.K.G. performed the data analysis and prepared the figures. J.K.G., P.G. and S.I.S. designed the study. A.M.B., K.L.F., S.H., D.M.L, S.I.S. and P.G. reviewed and edited the manuscript.

Competing interests The authors declare no competing interests.

Additional information
Extended data is available for this paper at https://doi.org/10.1038/s41586-018-0848-x.
Supplementary information is available for this paper at https://doi.org/10.1038/s41586-018-0848-x.
Reprints and permissions information is available at http://www.nature.com/reprints.
Correspondence and requests for materials should be addressed to J.K.G.
Publisher's note: Springer Nature remains neutral with regard to jurisdictional claims in published maps and institutional affiliations.

METHODS

GLACE-CMIP5. GLACE-CMIP5[7] is a multi-model series of experiments inspired by the original GLACE experiment[33] and designed to investigate land–atmosphere feedbacks along with climate change from 1950–2100. For each model, GLACE-CMIP5 simulations include: (1) until 2005, a reference run (CTL) based on the CMIP5 historic run; thereafter, the high-emission business-as-usual RCP8.5 scenario, which accounts for both the indirect impacts of soil moisture and the direct impact of CO_2 fertilization; (2) an experimental setup identical to that of CTL, but with soil moisture imposed as the mean climatology (that is, the seasonal cycle) from 1971–2000 throughout the study period (ExpA) to remove soil-moisture variability (short-term and inter-annual); and (3) an experimental setup identical to that of CTL, but with soil-moisture climatology imposed as a 30-year running mean (ExpB), to assess the impact of the trend in soil moisture (Extended Data Fig. 6).

The comparison of CTL and ExpB allows us to assess the impacts of soil-moisture variability on NBP; during negative anomalies this variability can cause vegetation water stress, resulting in reduced evapotranspiration, warmer temperatures and an increase in the ratio of autotrophic respiration (R_a) to GPP. The comparison of ExpB and ExpA isolates the effects of long-term soil-moisture changes, which can also induce vegetation water stress and increases in temperature and R_a/GPP if the vegetation cannot adapt quickly enough. The NBP time series of a third experiment (setup identical to that of CTL, but without the effects of carbon fertilization) are examined for trends to ensure that our results are in carbon equilibrium. The NBP includes carbon fluxes due to net primary production and to land use and land cover change (LULC).

Whereas six modelling groups participated in GLACE-CMIP5, four stored information on NBP for ExpA and ExpB and their results are used in this analysis (Extended Data Table 1). Multi-model means of NBP are used for the main results to increase robustness. It should be noted that among the four models only CESM includes the effects of nitrogen limitation on carbon uptake in its carbon-cycle model, and results in the Earth as a carbon source by the end of the twenty-first century (hence the negative spread in the inset of Fig. 1). However, it has been shown that this version (Community Land Model 4.0) overestimates the nitrogen limitation[34]. All of the data analysis and figure generation for this study were performed in MATLAB.

Isolating the effects of soil moisture. To isolate the effects of soil moisture on NBP changes, we adapt an approach from ref. [35]:

$$\Delta NBP_{land} = \Delta NBP_{SMvar} + \Delta NBP_{SMtrend} + \Delta NBP_{other} + \varepsilon \quad (1)$$

Here, each term is expressed as the corresponding influence on NBP (ΔNBP_{land}), where ΔNBP_{SMvar} is the change in NBP due to soil-moisture variability, $\Delta NBP_{SMtrend}$ is due to a change in mean soil-moisture state and ΔNBP_{other} is due to CO_2 fertilization and changes in temperature. The term ε accounts for all other limiting and contributing factors to NBP.

Using monthly data from the multi-model GLACE-CMIP5 simulations[9], CTL, ExpA and ExpB can be used to isolate the different contributions to ΔNBP due to soil-moisture variability $\Delta NBP_{SMvar} = \Delta NBP_{CTL-ExpB}$ and a soil moisture trend of $\Delta NBP_{SMtrend} = \Delta NBP_{ExpB-ExpA}$:

$$\Delta NBP_{CTL} = \Delta NBP_{CTL-ExpB} + \Delta NBP_{ExpB-ExpA} + \Delta NBP_{other} + \varepsilon \quad (2)$$

The results from this equation breakdown are used to create Figs. 1, 4. Similarly, Extended Data Figs. 1, 2, 4 are generated using the same approach, but investigate the effects of soil moisture on temperature, GPP and R_a. Extended Data Figs. 1, 4 use the RCP8.5 GPP and respiration data from the IPSL model owing to limited data availability. For the same reason, autotrophic respiration from the GLACE-CMIP5 experiments is used in lieu of ecosystem respiration.

Biosphere photosynthetic activity response curves: models. For the curves of GPP and R_a versus soil moisture (Fig. 2, Extended Data Fig. 5), monthly growing-season data are used. The growing season is defined for each pixel as the months in which the climatological mean is greater than or equal to half of the climatological maximum. For GPP and respiration, each pixel is normalized by its maximum value for better comparability. For soil moisture, owing to large differences in magnitude between models[36] and within the same model between regions, each pixel is standardized by its minimum value in time and its standard deviation in space for easier comparison.

To ensure that the growing season defined is representative of the entire data record, a second analysis is performed in which the growing season for each year is defined as the months in which the climatological mean is greater than or equal to half of a climatological maximum calculated from a 30-year mean. This does not change the nonlinear relationship between soil moisture and GPP seen in Fig. 2.

Biosphere photosynthetic activity response curves: observations. For the observational curve in Fig. 2, SIF data from the Global Ozone Monitoring Experiment-2 (GOME-2)[37] are used to represent photosynthetic activity, whereas TWS data from GRACE[38] are used to represent soil-water availability. As in the model analysis, monthly growing-season data are used, defined for each pixel as the months in which the climatological mean is greater than or equal to half of the climatological maximum.

SIF is a flux byproduct of photosynthesis that is mechanistically linked to photosynthesis[39] and has been shown to have a near-linear relationship with ecosystem GPP at the monthly and ecosystem scales[40–42]. On the basis of this relation, it has been successfully used as a proxy for GPP for numerous applications[32,43] and is used in this study as an indicator of biosphere activity. As with the model GPP data, the SIF data are normalized by their maximum value in time. The SIF data are detrended using a convolution to account for signal deterioration over the lifetime of the satellite.

The TWS from GRACE is derived from the sum of soil moisture, groundwater, surface water, snow and ice; it has been successfully used as a drought and vegetation activity indicator in previous studies[44,45]. In this application it is used as a proxy for soil-water availability. GRACE data are standardized using the same approach as that used for the model analysis of soil-moisture data (each pixel is standardized by its minimum value in time and its standard deviation in space).

This observational analysis, which is based on global remote-sensing products, confirms the asymmetric relationship between photosynthetic activity and water availability, as well as the sharp drop in photosynthetic activity at low water contents, which is qualitatively similar to the functional dependence of photosynthesis on soil moisture represented in the models. As a result, losses in carbon due to decreased photosynthesis during dry anomalies are not compensated by a similar-magnitude positive anomaly.

CO_2 fertilization experimental setup. To isolate the effects of CO_2 fertilization on NBP (Extended Data Fig. 9), data from the CMIP5 experiment ESMFixclim1 are used. ESMFixclim1 is an idealized experiment initialized as the pre-industrial control, in which the carbon cycle shows a 1% rise in atmospheric CO_2 concentration per year, whereas radiation is at pre-industrial levels[46]; seven models are available for this experiment: CanESM2, CESM1-BGC, HadGEM2-ES, IPSL-CM5A-LR, MPI-ESM-LR, MRI-ESM1 and NorESM1-ME. Although we use the years with atmospheric CO_2 concentration equivalent to that of 1950–2100 in RCP8.5, the experimental setups of ESMFixclim1 and RCP8.5 have differences that are not only related to the CO_2 concentration rate increase, but also to the lack of LULC and aerosols. Because of these differences in setup, Extended Data Fig. 9 is presented to show general NBP trends due to carbon fertilization, but the magnitudes reported should not be compared directly to the soil-moisture results.

Data availability

The GLACE-CMIP5 simulations are available from S.I.S. (sonia.seneviratne@ethz.ch) and the climate modelling groups upon reasonable request. All other data supporting the findings of this study are freely available from the following locations: CMIP5 model data, https://pcmdi.llnl.gov/; GOME-2 SIF data, ftp://ftp.gfz-potsdam.de/home/mefe/GlobFluo/GOME-2/gridded/; GRACE TWS data, https://grace.jpl.nasa.gov/data/get-data/; Atmospheric Infrared Sensor temperature and relative humidity data, https://airs.jpl.nasa.gov/data/get_data.

33. Koster, R. D. et al. Regions of strong coupling between soil moisture and precipitation. *Science* **305**, 1138–1140 (2004).
34. Oleson, K. W. et al. *Technical description of version 4.0 of the Community Land Model (CLM)*. NCAR Technical Note NCAR/TN-503+STR (2013); http://dx.doi.org/10.5065/D6RR1W7M.
35. Friedlingstein, P. et al. Climate–carbon cycle feedback analysis: results from the C^4MIP model intercomparison. *J. Clim.* **19**, 3337–3353 (2006).
36. Koster, R. D. et al. On the nature of soil moisture in land surface models. *J. Clim.* **22**, 4322–4335 (2009).
37. Köhler, P., Guanter, L. & Joiner, J. A linear method for the retrieval of sun-induced chlorophyll fluorescence from GOME-2 and SCIAMACHY data. *Atmos. Meas. Tech.* **8**, 2589–2608 (2015).
38. Watkins, M. M., Wiese, D. N., Yuan, D., Boening, C. & Landerer, F. W. Improved methods for observing Earth's time variable mass distribution with GRACE using spherical cap mascons. *J. Geophys. Res. Solid Earth* **120**, 2648–2671 (2015).
39. Porcar-Castell, A. et al. Linking chlorophyll a fluorescence to photosynthesis for remote sensing applications: mechanisms and challenges. *J. Exp. Bot.* **65**, 4065–4095 (2014).
40. Guanter, L. et al. Retrieval and global assessment of terrestrial chlorophyll fluorescence from GOSAT space measurements. *Remote Sens. Environ.* **121**, 236–251 (2012).
41. Frankenberg, C. et al. New global observations of the terrestrial carbon cycle from GOSAT: Patterns of plant fluorescence with gross primary productivity. *Geophys. Res. Lett.* **38**, L17706 (2011).
42. Joiner, J. et al. Global monitoring of terrestrial chlorophyll fluorescence from moderate spectral resolution near-infrared satellite measurements: methodology, simulations, and application to GOME-2. *Atmos. Meas. Tech.* **6**, 3883–3930 (2013).

43. Sun, Y. et al. OCO-2 advances photosynthesis observation from space via solar-induced chlorophyll fluorescence. *Science* **358**, eaam5747 (2017).
44. Jiang, W. et al. Annual variations of monsoon and drought detected by GPS: a case study in Yunnan, China. *Sci. Rep*. **7**, 1–10 (2017).
45. Yang, Y. et al. GRACE satellite observed hydrological controls on interannual and seasonal variability in surface greenness over mainland Australia. *J. Geophys. Res. Biogeosci*. **119**, 2245–2260 (2014).
46. Taylor, K. E., Stouffer, R. J. & Meehl, G. A. An overview of CMIP5 and the experiment design. *Bull. Am. Meteorol. Soc*. **93**, 485–498 (2012).
47. Neale, R. B. et al. The mean climate of the Community Atmosphere Model (CAM4) in forced SST and fully coupled experiments. *J. Clim*. **26**, 5150–5168 (2013).
48. Lawrence, D. M. et al. Parameterization improvements and functional and structural advances in version 4 of the Community Land Model. *J. Adv. Model. Earth Syst*. **3**, 1–27 (2011).
49. Dunne, J. P. et al. GFDL's ESM2 global coupled climate–carbon Earth system models. Part I: physical formulation and baseline simulation characteristics. *J. Clim*. **25**, 6646–6665 (2012).
50. Dunne, J. P. et al. GFDL's ESM2 global coupled climate–carbon Earth system models. Part II: carbon system formulation and baseline simulation characteristics. *J. Clim*. **26**, 2247–2267 (2013).
51. Milly, P. C. et al. An enhanced model of land water and energy for global hydrologic and Earth-system studies. *J. Hydrometeorol*. **15**, 1739–1761 (2014).
52. Dufresne, J.-L. et al. Climate change projections using the IPSL-CM5 Earth System Model: from CMIP3 to CMIP5. *Clim. Dyn*. **40**, 2123–2165 (2013).
53. Hourdin, F. et al. Impact of the LMDZ atmospheric grid configuration on the climate and sensitivity of the IPSL-CM5A coupled model. *Clim. Dyn*. **40**, 2167–2192 (2013).
54. Chéruy, F. et al. Combined influence of atmospheric physics and soil hydrology on the simulated meteorology at the SIRTA atmospheric observatory. *Clim. Dyn*. **40**, 2251–2269 (2013).
55. Stevens, B. et al. Atmospheric component of the MPI-M Earth System Model: ECHAM6. *J. Adv. Model. Earth Syst.* **5**, 146–172 (2013).
56. Hagemann, S., Loew, A. & Andersson, A. Combined evaluation of MPI-ESM land surface water and energy fluxes. *J. Adv. Model. Earth Syst*. **5**, 259–286 (2013).
57. Raddatz, T. J. et al. Will the tropical land biosphere dominate the climate–carbon cycle feedback during the twenty- first century? *Clim. Dyn*. **29**, 565–574 (2007).
58. Brovkin, V., Raddatz, T., Reick, C. H., Claussen, M. & Gayler, V. Global biogeophysical interactions between forest and climate. *Geophys. Res. Lett.* **36**, L07405 (2009).

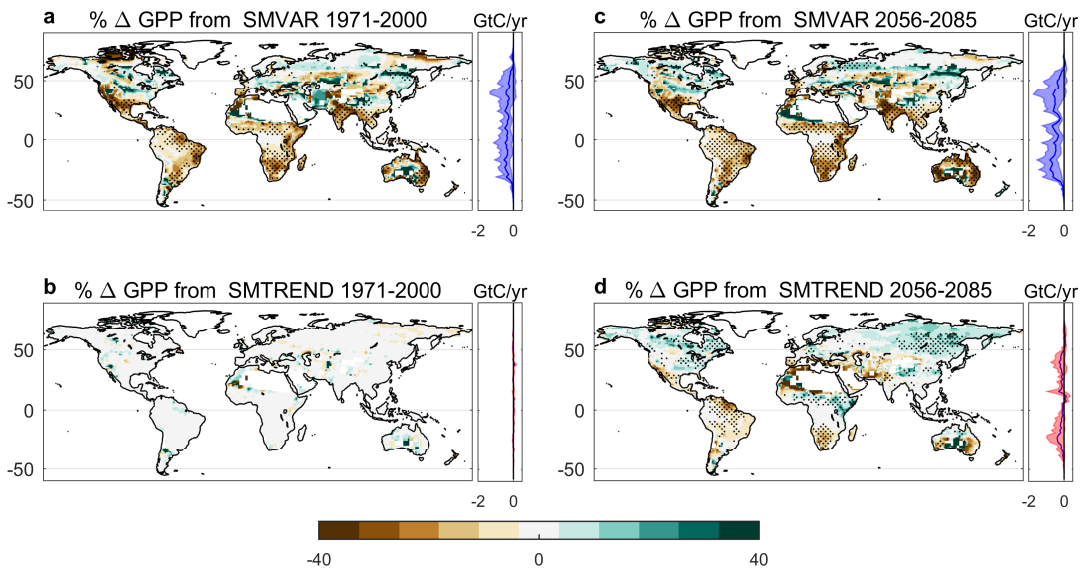

Extended Data Fig. 1 | Regional GPP changes. a–d, Per cent changes in GPP due to soil-moisture variability and trend during the baseline (1971–2000; **a**, **b**) and a future period (2056–2085; **c**, **d**). Stippling highlights regions where the three models agree on the sign of the change. The latitudinal GPP subplots on the right show how these changes translate to an overall GPP magnitude across latitudes. The thick line in each subplot represents the model mean and the shaded areas show the model spread.

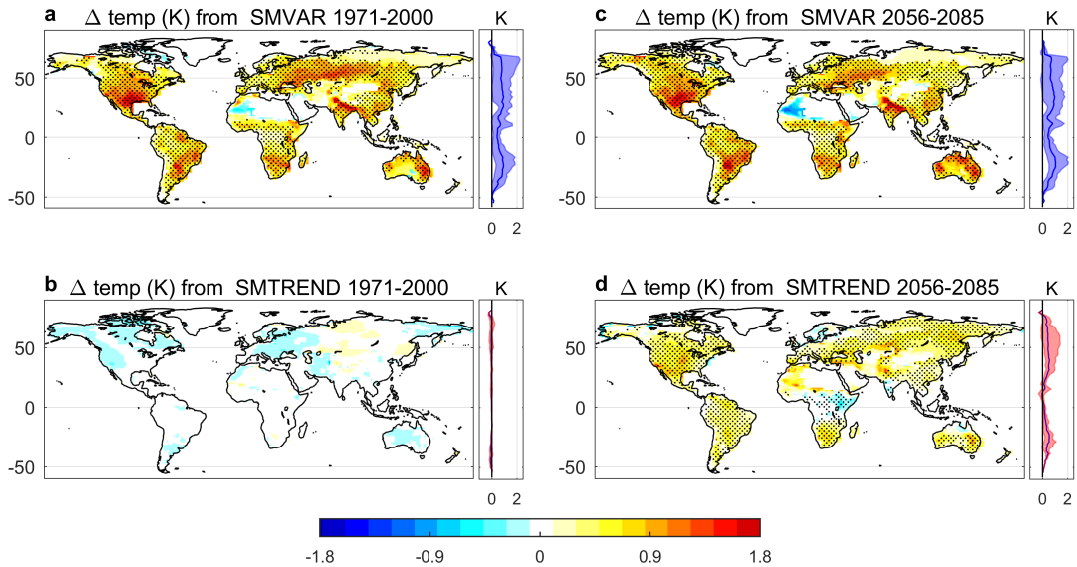

Extended Data Fig. 2 | Regional temperature changes. a–d, Temperature changes (in kelvins) due to soil-moisture variability and trend during the baseline (1971–2000; **a**, **b**) and a future modelled period (2056–2085; **c**, **d**). Stippling represents regions where at least three of the four models agree on the sign of the change. The latitudinal temperature subplots on the right show how these regional changes translate to a temperature change across latitudes. The thick lines in each subplot represent the model mean and the shaded areas show the model spread.

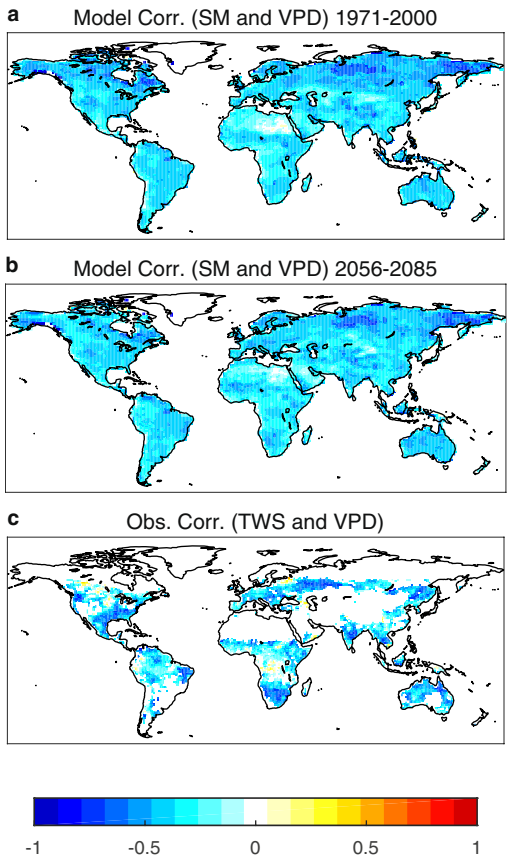

Extended Data Fig. 3 | Correlations between soil-water availability and VPD. a, **b**, Mean correlations between soil moisture and VPD during the baseline period (1971–2000; **a**) and in the future (2056–2085; **b**) from multi-model GLACE-CMIP5 simulations for the CTL run. **c**, Correlation between monthly TWS GRACE data and VPD data from the Atmospheric Infrared Sensor for the period 2007–2016. Monthly growing-season data are used, obtained from SIF observations or GPP simulations with values greater than half of the maximum climatology per pixel, and seasonal cycles were removed before determining the correlations.

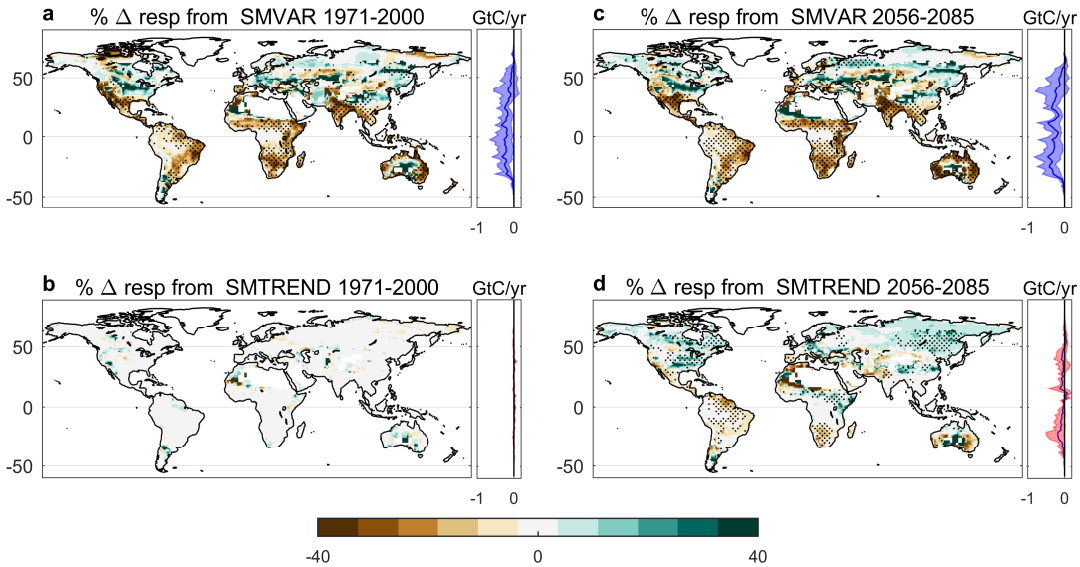

Extended Data Fig. 4 | Regional autotrophic respiration changes. **a**–**d**, Per cent changes in autotrophic respiration due to soil-moisture variability and trend during the baseline (1971–2000; **a**, **b**) and a future modelled period (2056–2085; **c**, **d**). Stippling represents regions where the three models agree on the sign of the change. The latitudinal respiration subplots on the right show how these changes translate to an overall respiration magnitude across latitudes. The thick line in each subplot represents the model mean and the shaded areas show the model spread.

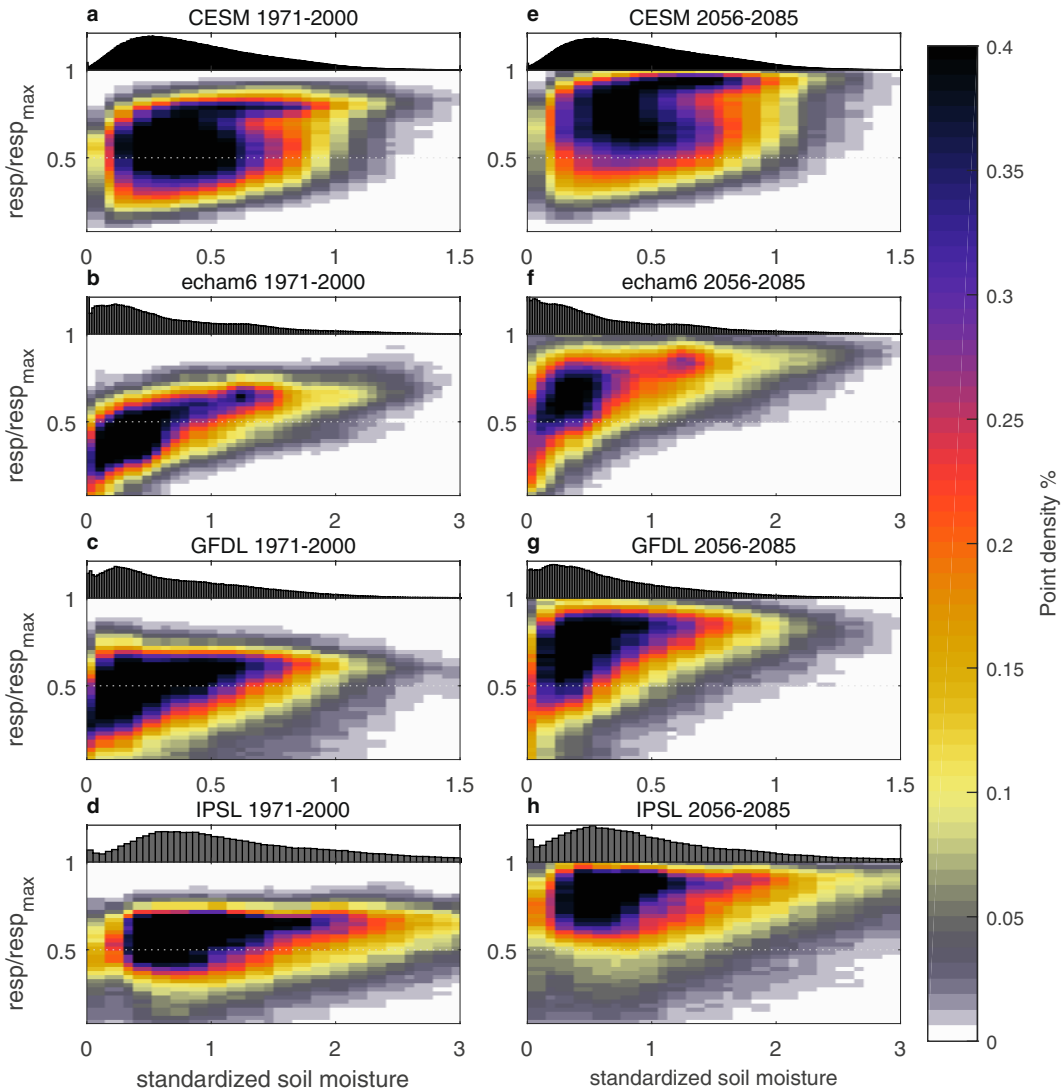

Extended Data Fig. 5 | Autotrophic respiration response curves. **a**–**h**, Normalized growing-season autotrophic respiration versus standardized soil moisture for the baseline (1971–2000; **a**–**d**) and a future period (2056–2085; **e**–**h**) in the GLACE-CMIP5 reference scenario. Details of the normalization and standardizations can be found in Methods. The probability density functions of the soil-moisture data are plotted at the top.

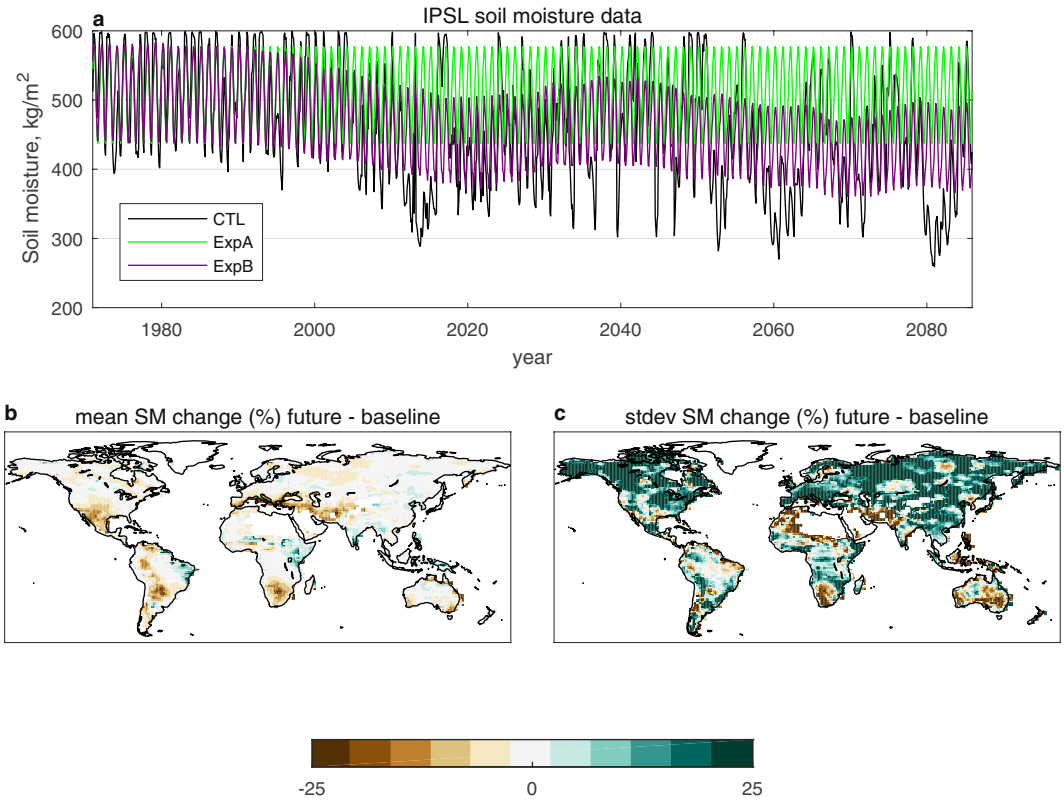

Extended Data Fig. 6 | GLACE-CMIP5 soil-moisture data. a, Monthly soil-moisture data from the GLACE-CMIP5 experiment for a pixel in Central Mexico, obtained using the IPSL model over the twenty-first century. CTL represents the RCP8.5 soil moisture, whereas ExpA uses the mean climatology of soil moisture from 1971–2000 and ExpB assumes soil moisture to be the 30-year running mean through the twenty-first century. **b**, Per cent change in mean soil moisture between the future and baseline periods in CTL, averaged across the four GLACE-CMIP5 models. **c**, Per cent change in soil-moisture variability between the future and baseline periods in CTL, averaged across the four GLACE-CMIP5 models.

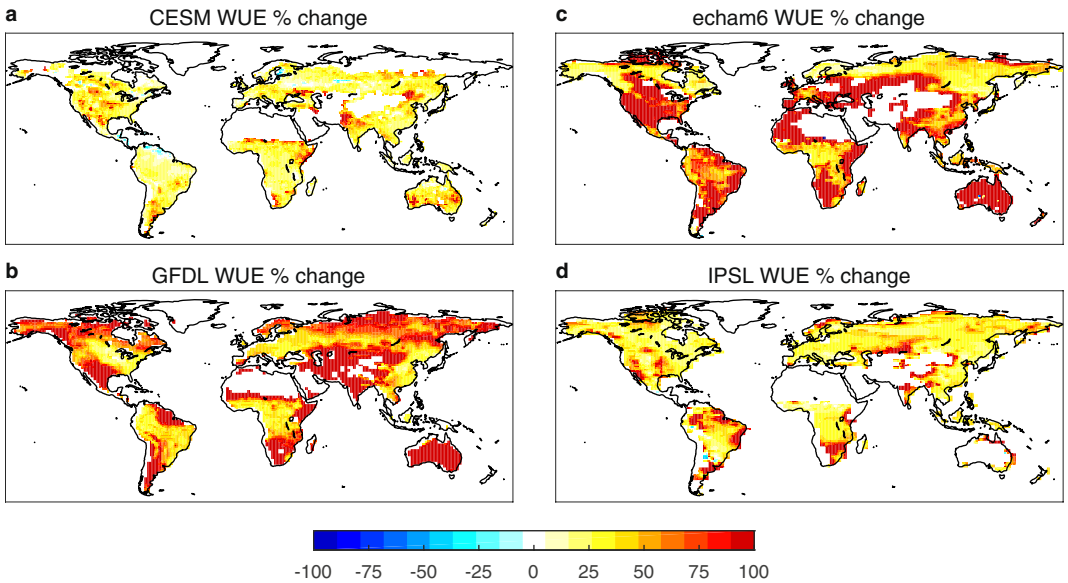

Extended Data Fig. 7 | Water-use efficiency changes. a–d, Per cent change in water-use efficiency (WUE) between the future (2056–2085) and baseline (1971–2000) periods for the CTL run, obtained using the CESM (**a**), GFDL (**b**), echam6 (**c**) and the IPSL (**d**) models. The WUE is calculated from GPP and evapotranspiration data. The IPSL GPP data are obtained using the RCP8.5 scenario, on which the CTL run is based.

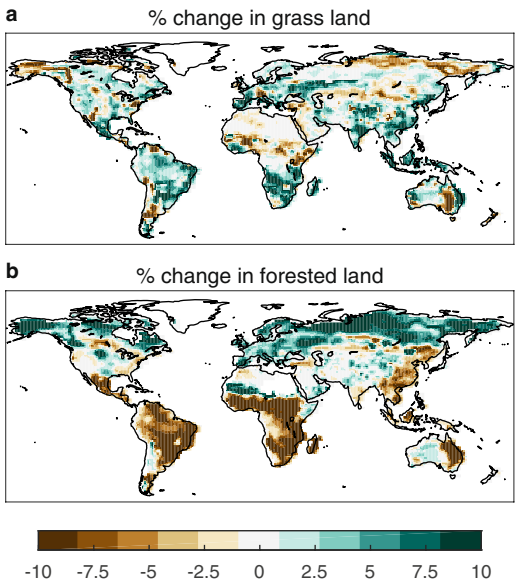

Extended Data Fig. 8 | Change in land-cover types. a, **b**, Multi-model mean per cent change between the future (2056–2085) and baseline (1971–2000) periods for grassland (**a**) and forested land (**b**). No data were available for the CESM model in this analysis.

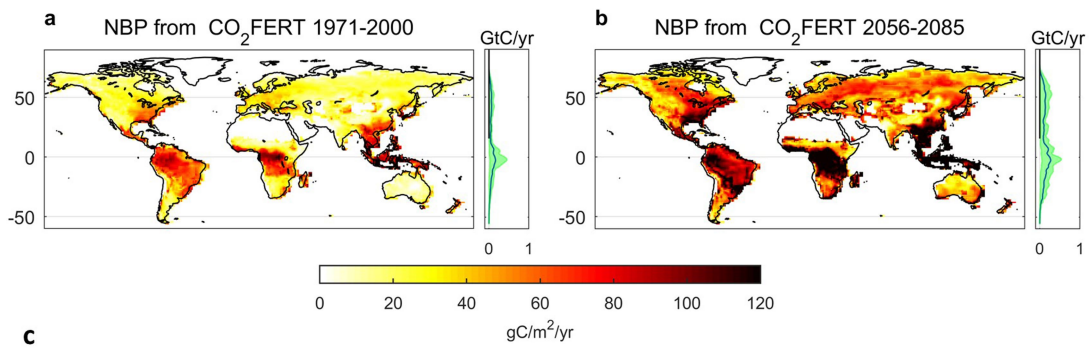

c

Modeling Center (or Group)	Institute ID	Model Name
Canadian Centre for Climate Modelling and Analysis	CCCMA	CanESM2
Community Earth System Model Contributors	NSF-DOE-NCAR	CESM1-BGC
Met Office Hadley Centre (additional HadGEM2-ES realizations contributed by Instituto Nacional de Pesquisas Espaciais)	MOHC (additional realizations by INPE)	HadGEM2-ES
Institut Pierre-Simon Laplace	IPSL	IPSL-CM5A-LR
Max-Planck-Institut für Meteorologie (Max Planck Institute for Meteorology)	MPI-M	MPI-ESM-LR
Meteorological Research Institute	MRI	MRI-ESM1
Norwegian Climate Centre	NCC	NorESM1-ME

Extended Data Fig. 9 | CO_2 fertilization effects on NBP. a–**c**, Regional and latitudinal changes in NBP during the baseline (1971–2000; **a**) and a future period (2056–2085; **b**) due to the effects of CO_2 fertilization. The maps are based on the results of seven CMIP5 models for the ESMFixClim1 scenario (**c**).

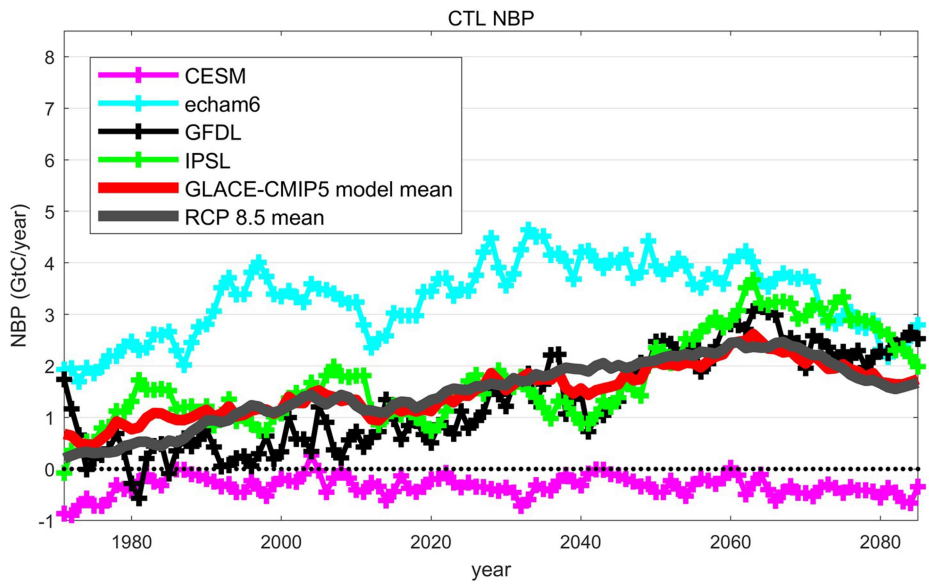

b

Modeling Center (or Group)	Institute ID	Model Name
Canadian Centre for Climate Modelling and Analysis	CCCMA	CanESM2
National Center for Atmospheric Research	NCAR	CCSM4
Community Earth System Model Contributors	NSF-DOE-NCAR	CESM1-CAM5
NOAA Geophysical Fluid Dynamics Laboratory	NOAA GFDL	GFDL-ESM2G GFDL-ESM2M
Met Office Hadley Centre (additional HadGEM2-ES realizations contributed by Instituto Nacional de Pesquisas Espaciais)	MOHC (additional realizations by INPE)	HadGEM2-CC HadGEM2-ES
Institute for Numerical Mathematics	INM	INM-CM4
Institut Pierre-Simon Laplace	IPSL	IPSL-CM5A-LR IPSL-CM5A-MR IPSL-CM5B-LR
Japan Agency for Marine-Earth Science and Technology, Atmosphere and Ocean Research Institute (The University of Tokyo), and National Institute for Environmental Studies	MIROC	MIROC-ESM MIROC-ESM-CHEM
Max-Planck-Institut für Meteorologie (Max Planck Institute for Meteorology)	MPI-M	MPI-ESM-LR MPI-ESM-MR
Meteorological Research Institute	MRI	MRI-ESM1
Norwegian Climate Centre	NCC	NorESM1-ME

Extended Data Fig. 10 | GLACE-CMIP5 predictions for CTL NBP. **a**, NBP through the twenty-first century for the CTL runs, as predicted by the GLACE-CMIP5 models listed in Extended Data Table 1. The multi-model mean value of the GLACE-CMIP5 runs, and the multi-model mean of 17 CMIP5 models from RCP8.5 are also displayed. **b**, Details of the modelling centre, institute and model used for each of the 17 CMIP5 models used to calculate the RCP8.5 mean.

Extended Data Table 1 | GLACE-CMIP5 model information

ESM Acronym	Atmospheric Model	Land Surface Model	References
CESM	National Center for Atmospheric Research Community Atmospheric Model (CAM4)	Community Land Model (CLM4)	Neale et al. [2013][47] Lawrence et al. [2011][48]
GFDL	Geophysical Fluid Dynamics Laboratory (GFDL) Earth System Model 2 (ESM2)	Land Model 3.0 (LM3.0)	Dunne et al. [2012; 2013][49,50] Milly et al. [2014][51]
IPSL*	Laboratoire de Météorologie Dynamique atmospheric model (LMDZ5A)	Organizing Carbon and Hydrology in Dynamic Ecosystems (ORCHIDEE; with two-layer soil hydrology scheme)	Dufresne et al. [2013][52] Hourdin et al. [2013][53] Chéruy et al. [2013][54]
MPI-ESM (echam6)	European Centre/Hamburg forecast system	Jena Scheme for Biosphere- Atmosphere Coupling in Hamburg (JSBACH)	Stevens et al. [2013][55] Hagemann et al. [2013][56] Raddatz et al. [2007][57] Brovkin et al. [2009][58]

Table adapted from ref. [9], Wiley.

*In plots of GPP and respiration from the GLACE-CMIP5 CTL run (Figs. 2, 3, Extended Data Figs. 1, 4, 5, 7), results for the IPSL model are based on RCP8.5. Results from IPSL are not included in the GPP and respiration results that require manipulation of ExpA and ExpB from the GLACE-CMIP5 experiments owing to limited data availability. It is unlikely that this should change the results substantially.